Journal of Thermal Analysis and Calorimetry (2023) 148:13281–13295
https://doi.org/10.1007/s10973-023-12647-7

Physicochemical processes and thermochemical parameters of $GdFeO_3$ formation from amorphous hydroxides: decisive role of carbonate impurities

Yamen Albadi[1,2] · Anastasia K. Bachina[3] · Vadim I. Popkov[3]

Received: 3 May 2023 / Accepted: 30 September 2023 / Published online: 21 November 2023

Abstract
The mechanism of formation of nanocrystalline gadolinium orthoferrite ($GdFeO_3$) during the heat treatment of gadolinium and iron(III) hydroxides synthesized by ultrasound-assisted co-precipitation was studied. The obtained samples were investigated by energy-dispersive X-ray spectroscopy, simultaneous thermal analysis via coupled differential scanning calorimetry and thermogravimetric analysis (DSC–TGA), powder X-ray diffraction (PXRD) and Fourier-transform infrared (FTIR) spectroscopy. The DSC–TGA results confirm that the formation of $GdFeO_3$ occurs after the complete decomposition of gadolinium oxycarbonate derivatives. The PXRD results indicate that $GdFeO_3$ is formed as a result of the reaction of amorphous iron(III) oxide (*am*-Fe_2O_3) at temperatures of 675–700 °C with amorphous gadolinium oxide (*am*-Gd_2O_3) (primary carbonate-independent pathway) and at temperatures of 725–775 °C with cubic gadolinium oxide (*c*-Gd_2O_3) transformed from the hexagonal gadolinium oxide (*h*-Gd_2O_3) which results from the decomposition of gadolinium oxycarbonate derivatives at temperatures of 675–725 °C (secondary carbonate-dependent pathway). The FTIR results are consistent with the assumption that gadolinium oxycarbonate derivatives decompose with the formation of *h*-Gd_2O_3 in the last-mentioned temperature range. The enthalpy of the reaction of formation of nanocrystalline $GdFeO_3$ defined from the DSC–TGA data is equal to -16.89 ± 0.36 kJ mol^{-1}. The activation energy for the formation of nanocrystalline $GdFeO_3$ obtained from the DSC data is equal to 1193.62 ± 112.05 kJ mol^{-1}, 1202.27 ± 112.06 kJ mol^{-1} and 1151.08 ± 106.53 kJ mol^{-1} according to the Kissinger, Augis–Bennett/Boswell and Flynn–Wall–Ozawa methods, respectively. Also, based on the DSC data, the true onset temperature of the formation of nanocrystalline $GdFeO_3$ was found to be ~ 756 °C.

Keywords Gadolinium orthoferrite · $GdFeO_3$ · Co-precipitation · Gadolinium oxycarbonates · Enthalpy of formation · Activation energy

Introduction

Rare-earth orthoferrites (*RE*FeO_3, where *RE* is a rare-earth element: Sc, Y, La–Lu) are a class of chemical compounds with an orthorhombic perovskite structure that have been actively studied due to their magnetic, optical and electrical properties [1–7]. One of these compounds is gadolinium orthoferrite ($GdFeO_3$) which has been proposed for various applications such as catalysis [8], photocatalysis [9], electrocatalysis [10], luminescence [11], gas sensing [12] and as a contrast agent for magnetic resonance imaging (MRI) [13–16]. In the synthesis of $GdFeO_3$ nanocrystals, various methods have been employed, including co-precipitation [17], hydrothermal method [18], solution combustion [19], sol–gel [20], microwave method [21], sonochemical method [22] and using heterobimetallic [23] and metal–organic [24] precursors. The co-precipitation method, which we preferred in our previous works [25–30], makes it possible to synthesize nanocrystalline $GdFeO_3$ with minimal foreign chemical impurities since the co-precipitated gadolinium and iron(III) hydroxides are dehydrated during heat treatment with the formation of the corresponding oxides, which then form the compound of interest. However, due to the active sorption of

✉ Yamen Albadi
albadi.yamen@technolog.edu.ru

1 Saint Petersburg State Institute of Technology, Saint Petersburg, Russian Federation 190013

2 Al-Baath University, Homs, Syrian Arab Republic 77

3 Ioffe Institute, Saint Petersburg, Russian Federation 194021

carbon oxide (CO_2) from the ambient air into the reagent solutions during their preparation or onto the surface of co-precipitated hydroxides during their washing and drying, gadolinium carbonate can be formed. Such partial carbonatization of co-precipitated hydroxides may lead to sample inhomogeneity in terms of phase composition, and as a result, to the formation of another phase along with $GdFeO_3$ after heat treatment [25, 26, 30]. Therefore, it is of scientific and practical interest to study and understand the role of carbonates in the formation mechanism of nanocrystalline $GdFeO_3$ by co-precipitation.

In the literature, several publications have investigated the mechanism of formation of $GdFeO_3$ nanocrystals by the co-precipitation method [31–33]. Prakash et al. [31] investigated the formation of nanocrystalline $GdFeO_3$ by sintering a synthesized sample of co-precipitated hydroxides at temperatures of 600–1200 °C. They found that gadolinium oxide (Gd_2O_3) was present in the sintered products up to a temperature of 1000 °C, above which single-phase $GdFeO_3$ nanocrystals were obtained; therefore, they consider the temperature of 1200 °C to be optimal for sintering. The authors reported the presence of carbonates in the synthesized sample, but they did not indicate their role in the formation of $GdFeO_3$. Tugova and Karpov [32] studied the mechanism of formation of nanocrystalline $GdFeO_3$ upon the calcination of co-precipitated hydroxides at temperatures of 500–900 °C. They established that the products heat treated at temperatures of 500–600 °C contain gadolinium dioxymonocarbonate ($Gd_2O_2CO_3$) which decomposes at temperatures of 600–700 °C to form cubic Gd_2O_3, and starting from a temperature of 700 °C, $GdFeO_3$ is formed. Based on these results, they concluded that the formation of $GdFeO_3$ nanocrystals occurs through two mechanisms: the first mechanism is related to the simultaneous dehydration of co-precipitated hydroxides, while the other is associated with both dehydration and decarbonation, which leads to an increase in the temperature of $GdFeO_3$ synthesis. The work of Popkov et al. [33] confirmed the results of the previous one [32] that the formation of $GdFeO_3$ nanocrystals proceeds via two routes: from the co-precipitated hydroxides along the main route and from the products of partial carbonatization along the side one.

In this paper, we continue the work of the aforementioned colleagues, focus on simultaneous thermal analysis of the precursor and study in detail the mechanism of formation of $GdFeO_3$ nanocrystals synthesized employing the ultrasound-assisted co-precipitation method, which apparently, maintains sample homogeneity by enhancing diffusion and mixing processes [30]. The content of carbonates in the products of heat treatment of the synthesized sample of co-precipitated hydroxides at different temperatures is estimated. In addition, the true onset temperature of the formation of nanocrystalline $GdFeO_3$ is found, and the enthalpy and the activation energy for this formation reaction are also defined.

Materials and methods

Synthesis of samples

In this work, gadolinium and iron(III) hydroxides were synthesized by direct co-precipitation accompanied by ultrasonication. After that, samples of the obtained co-precipitated hydroxides were heated at different temperatures in the air.

An aqueous solution of stoichiometric amounts of gadolinium nitrate hexahydrate "$Gd(NO_3)_3{\cdot}6H_2O$" (puriss., 99.9%) and iron(III) nitrate nonahydrate "$Fe(NO_3)_3{\cdot}9H_2O$" (pur., 98.00%) with a concentration of 0.01 mol L^{-1} for each salt was used as a source of gadolinium and iron(III) ions. An aqueous solution of sodium hydroxide (NaOH) (p.a.) with a concentration of 1 mol L^{-1} was used as a precipitating medium. Gadolinium and iron(III) nitrates react with sodium hydroxide to form water-soluble sodium nitrate ($NaNO_3$) and a precipitate of gadolinium hydroxide "$Gd(OH)_3$" and iron(III) hydroxide "$Fe(OH)_3$" (exchange reaction). The equation for this reaction can be written as follows:

$$Gd(NO_3)_3(aq) + Fe(NO_3)_3(aq) + 6NaOH(aq) = Gd(OH)_3(s) + Fe(OH)_3(s) + 6NaNO_3(aq).$$

Co-precipitation of gadolinium and iron(III) hydroxides

For the synthesis of co-precipitated hydroxides, 100 mL of 1 mol L^{-1} sodium hydroxide solution was added dropwise to 100 mL of 0.01 mol L^{-1} gadolinium and iron(III) nitrates solution, which was constantly stirred with a magnetic stirrer and irradiated with ultrasound by immersing the ultrasonic horn of a ''Venpan type UD-20 automatic'' ultrasonic disintegrator into it throughout the entire co-precipitation process. The synthesis was repeated two more times, each time with 100 mL of each reagent solution. Then, the resulting precipitates with the supernatants from the three syntheses were mixed using a magnetic stirrer. After settling, most of the supernatant was decanted, and the co-precipitated hydroxides were separated from the remainder by centrifugation. Thereafter, the obtained precipitate was washed three times with distilled water to remove residual sodium hydroxide and sodium nitrate. The washed co-precipitated hydroxides were separated from water by centrifugation and then dried at a temperature of 45 °C.

Heat treatment of co-precipitated hydroxides

Samples of the synthesized co-precipitated hydroxides with a mass of about 50 mg were heated at different temperatures in the range of 650–850 °C with an interval of 25 °C (650,

675, 700, 725, 750, 775, 800, 825 and 850 °C) for 4 h in the air.

Characterization of co-precipitated hydroxides

Energy-dispersive X-ray spectroscopy

The content of gadolinium and iron in the synthesized sample of co-precipitated hydroxides was determined by energy-dispersive X-ray spectroscopy (EDXS) using a "TESCAN VEGA3" scanning electron microscope (TESCAN ORSAY HOLDING, Brno-Kohoutovice, Czech Republic) with an accelerating voltage of 30.0 kV coupled with an "x-act" silicon drift detector (Oxford Instruments, Abingdon, Oxfordshire, UK).

Differential scanning calorimetry and thermogravimetric analysis

The synthesized sample of co-precipitated hydroxides was investigated by differential scanning calorimetry and thermogravimetric analysis (DSC–TGA) using a "NETZSCH STA 449 F3" simultaneous thermal analyzer (NETZSCH-Gerätebau GmbH, Selb, Germany) up to 900 °C at three different heating rates (10, 20 and 30 °C min^{-1}) in an inert atmosphere of argon. The sample masses were 11.160, 11.568 and 11.183 mg at heating rates of 10, 20 and 30 °C min^{-1}, respectively. The DSC and TGA curves of the reference substances (potassium chromate "K_2CrO_4" and barium carbonate "$BaCO_3$") were obtained using the same simultaneous thermal analyzer at the same three heating rates. The sample mass of K_2CrO_4 was 15.677 mg at a heating rate of 10 °C min^{-1} and 16.130 mg at heating rates of 20 and 30 °C min^{-1}, while the sample mass of $BaCO_3$ was 11.933 mg at all heating rates. All measurements were carried out in platinum crucibles (DSC/TG pan Pt). The processing of the DSC–TGA data was carried out using the "NETZSCH Proteus Thermal Analysis" software.

Characterization of heat-treated products

Powder X-ray diffraction

The powder X-ray diffraction (PXRD) patterns were recorded using a ''Rigaku SmartLab 3'' diffractometer (Rigaku Corporation, Tokyo, Japan) in the Bragg angle range of 15–61° at a scan speed of 0.2 deg min^{-1} and a step width of 0.01°. The processing of the PXRD data was carried out using the ''SmartLab Studio II'' software. The mass fractions of the crystalline phases were estimated by the Rietveld refinement method using the crystal structure data of the Inorganic Crystal Structure Database (ICSD) structures with the identifiers of ICSD 27278, ICSD 162247 and ICSD 150677 for orthorhombic $GdFeO_3$, hexagonal Gd_2O_3 and cubic Gd_2O_3, correspondently. The relative mass fractions of the X-ray amorphous phases in the products that underwent heat treatment at temperatures up to 775 °C were estimated by normalizing the obtained diffractograms of these products, determining the integrated intensity of the amorphous halo on the normalized diffraction patterns in the Bragg angle range of ~ 15.2–27.2° and recalculating the resulting values as percentages of the maximum. The estimated results of mass fractions of the X-ray amorphous and crystalline phases in each heat-treated product were combined by subtracting the integrated intensity of the amorphous halo from 100% and recalculating the mass fractions of crystalline phases as fractions of the obtained value.

Fourier-transform infrared spectroscopy

The Fourier-transform infrared (FTIR) spectra in the wavenumber range of 400–4000 cm^{-1} were obtained by Kubelka–Munk transformation of diffuse reflectance data acquired using a "Bruker INVENIO-S" FTIR spectrometer (Bruker Optics, Ettlingen, Germany) with a "PIKE" diffuse reflectance attachment (PIKE Technologies, Madison, WI, USA). The relative mass percentages of gadolinium oxycarbonate derivatives in the products that underwent heat treatment at temperatures up to 800 °C were estimated by normalizing the obtained FTIR spectra of these products, determining the integrated intensity of the asymmetric and symmetric stretching vibrations of carbonate groups (CO_3^{2-}) on the normalized FTIR spectra in the wavenumber range of ~ 1260–1625 cm^{-1} and recalculating the resulting values as percentages of the maximum.

Results and discussion

Energy-dispersive X-ray spectroscopy

According to the EDX spectrum presented in Fig. 1, the synthesized sample of co-precipitated hydroxides is practically chemically pure. The carbon detected in the investigated sample is related to the presence of carbonate groups, the appearance of which, as we mentioned earlier, is a consequence of the active sorption of CO_2 from the ambient air into the reagent solutions during their preparation or onto the surface of co-precipitated hydroxides during their washing and drying. Based on the EDXS results, the atomic ratio of gadolinium to iron (Gd:Fe) is $(49.92 \pm 0.03)\%$:$(50.08 \pm 0.03)\%$; therefore, the average Gd:Fe atomic ratio is about 1.000:1.003, which is very close to the atomic ratio of 1:1 in $GdFeO_3$, i.e., the content of gadolinium and iron in the synthesized sample corresponds to the stoichiometry of the compound of interest. It is worth noting that the

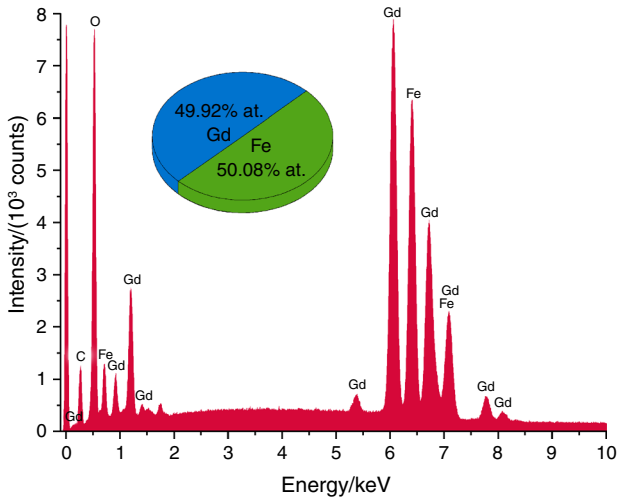

Fig. 1 EDX spectrum of the co-precipitated hydroxides. The inset (pie chart) shows the average Gd:Fe atomic ratio in the sample

Gd:Fe atomic ratio is preserved during the synthesis since neither gadolinium nor iron is included in the composition of compounds that are volatile during the heat treatment of co-precipitated hydroxides.

Differential scanning calorimetry and thermogravimetric analysis

As was shown earlier [25, 27, 29, 33], upon heat treatment, gadolinium and iron(III) hydroxides undergo a series of physicochemical processes before forming $GdFeO_3$. The DSC and TGA curves of the synthesized sample of co-precipitated hydroxides at different heating rates (10–30 °C min^{-1}) are presented in Fig. 2a and b, respectively. The first derivatives of the TGA curves (the DTG curves) are presented in supplementary Fig. S1. On the obtained DSC curves (Fig. 2a), 7 thermal effects can be detected: 6 endothermic (effects indicated by downward pointing arrows 1–6) and one exothermic (effect indicated by upward pointing arrow 8), whereas on the presented DTG curves (Fig. S1), 7 endothermic effects are observed (effects 1–7). These effects are associated with the evaporation of the physically adsorbed water on the sample surface (endothermic effect 1: ~ 53–63 °C by DSC, ~ 51–58 °C by DTG); the dehydration of iron(III) hydroxide to form iron(III) oxide (endothermic effect 2: ~ 126–163 °C by DSC, ~ 132–156 °C by DTG); the dehydration of gadolinium hydroxide in three stages: firstly to form gadolinium oxide sesquihydrate (endothermic effect 3: ~ 226–247 °C by DSC, ~ 223–246 °C by DTG), secondly to form gadolinium oxyhydroxide (endothermic effect 4: ~ 294–319 °C by DSC, ~ 299–322 °C by DTG), and thirdly, to gadolinium oxide (endothermic effect 6: ~ 414–452 °C by DSC, ~ 420–442 °C by DTG); the first stage of decomposition of gadolinium carbonate to form an oxycarbonate derivative (endothermic effect 5: ~ 371–384 °C by DSC, ~ 369–392 °C by DTG); the last stage of decomposition of gadolinium oxycarbonate derivative to form gadolinium oxide (endothermic effect 7: ~ 756–758 °C by DTG), and finally, the formation of gadolinium orthoferrite from gadolinium and iron(III) oxides (exothermic effect 8: ~ 764–772 °C by DSC). All these results are summarized in Table 1. As can be seen from Table 1, the temperatures of the maximum thermal and mass loss effects

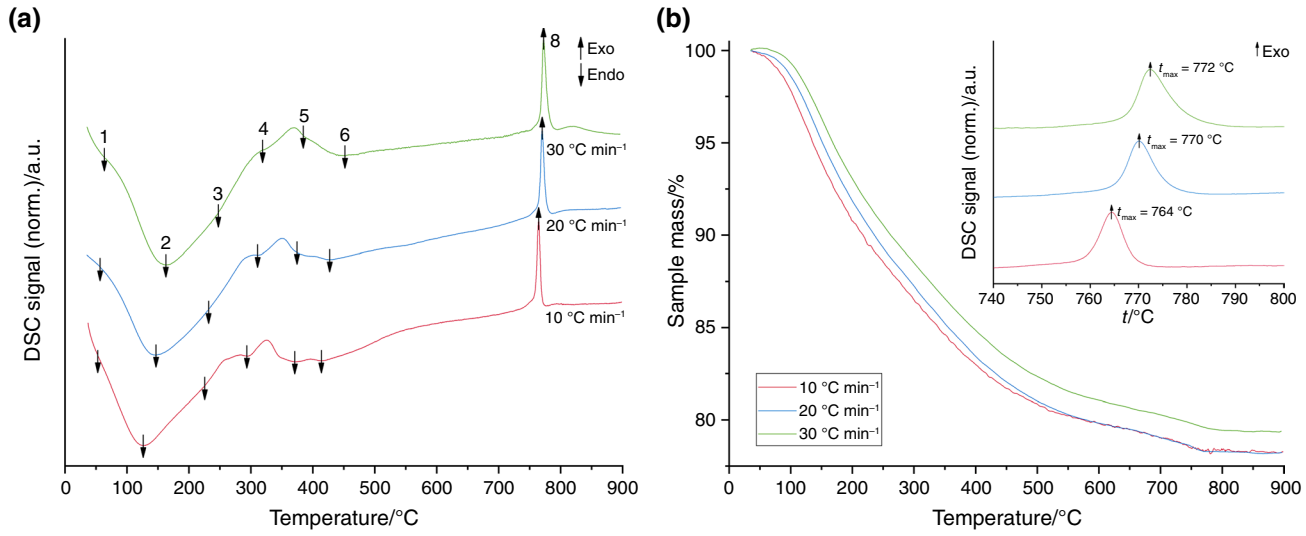

Fig. 2 DSC (**a**) and TGA (**b**) curves of the co-precipitated hydroxides at different heating rates. The inset in (**b**) shows the exothermic effect of $GdFeO_3$ formation (t is the temperature, t_{max} is the temperature of the maximum thermal effect). The arrows pointing down indicate endothermic effects (effects 1–6), while the arrows pointing up indicate exothermic effects (effect 8)

Table 1 Thermal (DSC) and mass loss (DTG) effects of the co-precipitated hydroxides at different heating rates

Effect no	Endo/exo	t_{max}/°C at $\beta = 10$ °C min^{-1}		at $\beta = 20$ °C min^{-1}		at $\beta = 30$ °C min^{-1}		Process [33]
		DSC	DTG	DSC	DTG	DSC	DTG	
1	Endo	53	51	57	58	63	58	$-H_2O$ (adsorbed)
2	Endo	126	135	147	132	163	156	$2Fe(OH)_3 = Fe_2O_3 + 3H_2O$
3	Endo	226	223	232	231	247	246	$2Gd(OH)_3 = Gd_2O_3 \cdot 1.5H_2O + 1.5H_2O$
4	Endo	294	299	311	313	319	322	$Gd_2O_3 \cdot 1.5H_2O = 2GdOOH + 0.5H_2O$
5	Endo	371	369	374	377	384	392	$Gd_2(CO_3)_3 = Gd_2O_{3-x}(CO_3)_x + (3-x)$ CO_2 [a]
6	Endo	414	420	427	429	452	442	$2GdOOH = Gd_2O_3 + H_2O$
7	Endo	[b]	756	[b]	758	[b]	756	$Gd_2O_{3-x}(CO_3)_x = Gd_2O_3 + xCO_2$ [a]
8	Exo	764	–	770	-	772	–	$Fe_2O_3 + Gd_2O_3 = 2GdFeO_3$

t_{max} is the temperature of the maximum thermal or mass loss effect, β is the heating rate

[a]The values of x in gadolinium oxycarbonate derivatives are defined later in this paper (see Section "Carbonate content in gadolinium oxycarbonate derivatives")

[b]These temperatures could not be accurately determined due to stage overlap and low intensity

generally tend to increase with increasing heating rate. According to the TGA curves (Fig. 2b), the total mass loss is about 21.69%, 21.75% and 20.58% at a heating rate of 10, 20 and 30 °C min^{-1}, correspondently. These mass losses are related to the release of water (effects 1–4 and 6) and CO_2 (effects 5 and 7). The results obtained are in good agreement with the previous ones [32, 33], which confirm that the formation of $GdFeO_3$ occurs after the mass loss is completed, i.e., after the complete decomposition of gadolinium oxycarbonate derivatives.

Enthalpy of the reaction of formation of nanocrystalline $GdFeO_3$

To found the enthalpy of formation of nanocrystalline $GdFeO_3$ based on the DSC–TGA results, two reference substances were used: K_2CrO_4 and $BaCO_3$. Potassium chromate and barium carbonate undergo certain physicochemical transformations at temperatures below and above the formation temperature of $GdFeO_3$, respectively. According to the data used to calibrate the thermal analyzer, at a heating rate of 10 °C min^{-1}, K_2CrO_4 transforms from orthorhombic to hexagonal form in an endothermic process [34] at a temperature of 668.0 °C with an enthalpy of 35.000 J g^{-1}, while $BaCO_3$ melts in an endothermic process at a temperature of 808.0 °C with an enthalpy of 94.900 J g^{-1}.

At each heating rate (β), the onset temperature (t_{onset}) and peak area (A) of the endothermic effects of the reference substances and the exothermic effect of $GdFeO_3$ formation were determined from the DSC curves, whereas the values of sample mass at each onset temperature (m_{onset}) were determined from the TGA curves. Peak areas in μV °C were calculated from their values in μV s given by the software using the heating rate according to Eq. 1.

$$A\left[\mu V^{\circ}C\right] = A\left[\mu V\,s\right] \cdot \frac{\beta\left[^{\circ}C\,min^{-1}\right]}{60\left[s\,min^{-1}\right]} \quad (1)$$

Then, the "specific" peak areas (A^*) were calculated by dividing the obtained peak areas by the corresponding sample masses at onset temperature as shown in Eq. 2.

$$A^*\left[\mu V^{\circ}C\,mg^{-1}\right] = \frac{A\left[\mu V^{\circ}C\right]}{m_{onset}\left[mg\right]} \quad (2)$$

After that, the known enthalpy values associated with the endothermic effects of the reference substances were divided by the corresponding "specific" peak areas as shown in Eq. 3.

$$\Delta H/A^*\left[J\mu V^{-1}\,^{\circ}C^{-1}\right] = \frac{\Delta H\left[Jg^{-1}\right] \cdot 10^{-3}\left[g\,mg^{-1}\right]}{A^*\left[\mu V\,^{\circ}C\,mg^{-1}\right]} \quad (3)$$

Then, the resulting values of $\Delta H/A^*$ were plotted as a function of t_{onset} at each heating rate (Fig. 3), where each dependence is a straight line drawn between two reference points: one for K_2CrO_4 and the other for $BaCO_3$.

Based on the equations of the straight lines obtained, the values of $\Delta H/A^*$ for $GdFeO_3$ at each heating rate were calculated using the corresponding onset temperatures of the exothermic effect of $GdFeO_3$ formation. All these data are summarized in Table 2.

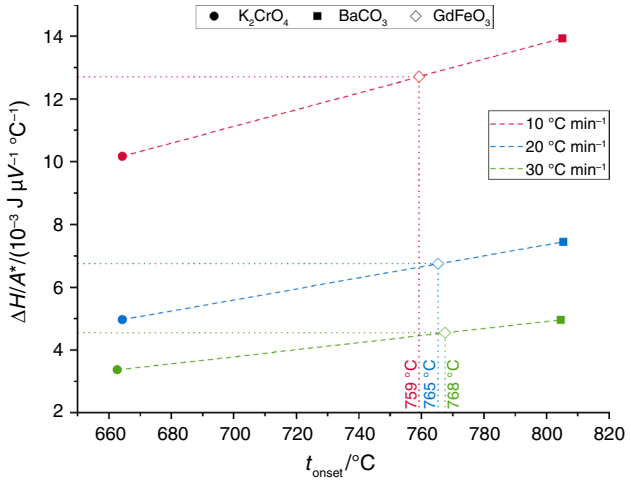

Fig. 3 Dependences of the ratio of enthalpy to the "specific" peak area on the onset temperature of the thermal effect in the temperature range ~ 663–805 °C at different heating rates

Thereafter, multiplying the resulting values of $\Delta H/A^*$ for $GdFeO_3$ at each heating rate by the corresponding "specific" peak areas calculated earlier by Eq. 2, the enthalpy of the reaction of formation of nanocrystalline $GdFeO_3$ can be estimated (Eq. 4).

$$\Delta H\left[\mathrm{J\,g^{-1}}\right] = \Delta H/A^*\left[\mathrm{J\mu V^{-1}\,°C^{-1}}\right] \cdot A^*\left[\mathrm{\mu V\,°C\,mg^{-1}}\right] \cdot 10^3\left[\mathrm{mg\,g^{-1}}\right] \quad (4)$$

According to Eq. 4, the enthalpy of the reaction of formation of nanocrystalline $GdFeO_3$ is in the range from about -63.36 to -66.54 J g^{-1} or from about -16.54 to -17.37 kJ mol^{-1}. In other words, it is approximately equal to -64.67 ± 1.36 J g^{-1} or -16.89 ± 0.36 kJ mol^{-1}. This value is much less than the enthalpy of formation of $GdFeO_3$ at 298.15 K (-1351.432 ± 8.368 kJ mol^{-1} [35]), which can be explained by the fact that the standard enthalpy of formation corresponds to the formation of $GdFeO_3$ from its constituent elements (Gd, Fe and O) in their standard states, while in this work, the enthalpy of formation of $GdFeO_3$ from gadolinium and iron(III) oxides was estimated. Furthermore, the calculated value does not correspond to bulk $GdFeO_3$, but to nanosized $GdFeO_3$; therefore, it should be smaller.

Activation energy for the formation of nanocrystalline $GdFeO_3$

To estimate the activation energy for the formation of nanocrystalline $GdFeO_3$ based on the DSC data, three kinetic methods were applied: the Kissinger method [36], the Augis–Bennett/Boswell method [37, 38] and the Flynn–Wall–Ozawa (FWO) method [39, 40]. These non-isothermal kinetic methods depend on the relationship between the heating rate and the absolute temperature at which the reaction reaches its maximum value [41]. The mathematical formulas for these methods can be written as shown in Eqs. 5–7.

Kissinger method

$$\ln\left(\frac{\beta}{T_{\max}^2}\right) = -\frac{E_a}{RT_{\max}} + \ln\left(\frac{AR}{E_a}\right) \quad (5)$$

Augis–Bennett/Boswell method

$$\ln\left(\frac{\beta}{T_{\max}}\right) = -\frac{E_a}{RT_{\max}} + \text{const.} \quad (6)$$

Flynn–Wall–Ozawa method

$$\left.\begin{aligned} \log\beta &= -0.4567\frac{E_a}{RT_{\max}} + \text{const.} \\ \ln\beta &= -1.052\frac{E_a}{RT_{\max}} + \text{const.} \end{aligned}\right\} \quad (7)$$

Table 2 DSC–TGA data used in the estimation of the enthalpy of the reaction of formation of nanocrystalline $GdFeO_3$

β/°C min^{-1}	Substance	t_{onset}/°C	m_{onset}/mg	A/μV s	A/μV °C	A^*/μV °C mg^{-1}	$\Delta H/A^*$/J μV^{-1} $°C^{-1}$
10	K_2CrO_4	664	15.610	322.2	53.70	3.44	1.02×10^{-2}
	$BaCO_3$	805	11.804	482.3	80.38	6.81	1.39×10^{-2}
	$GdFeO_3$	759	8.754	−261.8	−43.63	−4.98	$\mathbf{1.27\times10^{-2}}$
20	K_2CrO_4	664	16.330	345.2	115.1	7.05	4.97×10^{-3}
	$BaCO_3$	805	12.469	476.2	158.7	12.73	7.45×10^{-3}
	$GdFeO_3$	765	9.064	−268.1	−89.37	−9.86	$\mathbf{6.75\times10^{-3}}$
30	K_2CrO_4	663	16.720	346.9	173.5	10.37	3.37×10^{-3}
	$BaCO_3$	805	12.394	474.6	237.3	19.15	4.96×10^{-3}
	$GdFeO_3$	768	8.905	−251.3	−125.7	−14.11	$\mathbf{4.54\times10^{-3}}$

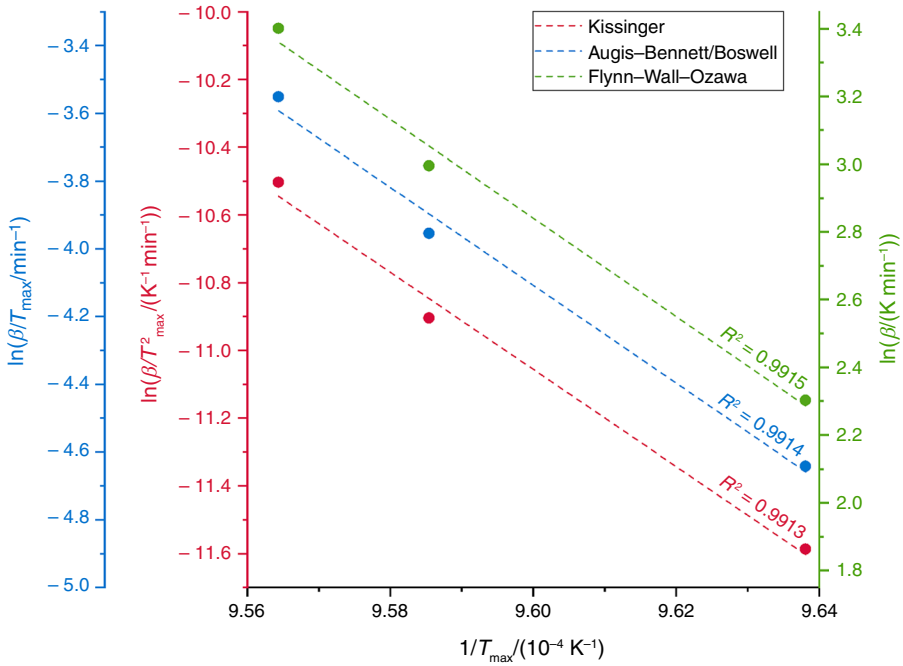

Fig. 4 Dependences of $\ln(\beta/T^2_{max})$ (Kissinger method), $\ln(\beta/T_{max})$ (Augis–Bennett/Boswell method) and $\ln \beta$ (FWO method) on the reciprocal absolute temperature of the maximum exothermic effect of $GdFeO_3$ formation on the DSC curves. R^2 is the coefficient of determination

In these equations, β is the heating rate, T_{max} is the absolute temperature at which the reaction reaches its maximum value, i.e., the peak of the thermal effect (in our work, T_{max} is the absolute temperature of the maximum exothermic effect of $GdFeO_3$ formation on the corresponding DSC curve), E_a is the activation energy, A is the pre-exponential factor and R is the molar gas constant.

Based on the Kissinger method (Eq. 5), plotting $\ln(\beta/T^2_{max})$ against $1/T_{max}$ results in a straight line with a slope of $-E_a/R$ and a y-intercept of $\ln(AR/E_a)$. Similarly, in accordance with the Augis–Bennett/Boswell method (Eq. 6), plotting $\ln(\beta/T_{max})$ versus $1/T_{max}$ gives a straight line with a slope of $-E_a/R$, whereas according to the FWO method (Eq. 7), plotting of $\ln \beta$ against $1/T_{max}$ gives a straight line with a slope of $-1.052E_a/R$. Figure 4 shows these straight lines obtained using the previously determined temperatures of the maximum exothermic effect of $GdFeO_3$ formation on the DSC curves at different heating rates (Table 1, effect 8). In the first two methods, the activation energy for the formation of nanocrystalline $GdFeO_3$ can be calculated by multiplying the resulting slopes by $-R$, while in the third method, the obtained slope should be multiplied by $-R$ and divided by 1.052. The DSC data used and the calculation results are summarized in Table 3.

According to the calculation results, the activation energy for the formation of nanocrystalline $GdFeO_3$ is approximately equal to 1193.62 ± 112.05 kJ mol^{-1}, 1202.27 ± 112.06 kJ mol^{-1} and 1151.08 ± 106.53 kJ mol^{-1}

Table 3 DSC data used in the estimation of activation energy for the formation of nanocrystalline $GdFeO_3$ and the results obtained

β/°C min^{-1}	t_{max}/°C	T_{max}/K	$1/T_{max}$/K^{-1}	Kissinger $\ln \beta/T^2_{max}$/ K^{-1} min^{-1}	Augis–Bennett/Boswell $\ln \beta/T_{max}$/min^{-1}	Flynn–Wall–Ozawa $\ln \beta$/ K min^{-1}
10	764	1037	9.64×10^{-4}	−11.59	−4.642	2.303
20	770	1043	9.59×10^{-4}	−10.90	−3.954	2.996
30	772	1045	9.56×10^{-4}	−10.50	−3.551	3.401
			R^2	0.9913	0.9914	0.9915
			E_a/ kJ mol^{-1}	1193.62	1202.27	1151.08
			ΔE_a/kJ mol^{-1}	112.05	112.06	106.53
			$\Delta E_a/E_a$/%	9.39	9.32	9.25

R^2 is the coefficient of determination, ΔE_a is the standard error of the calculated activation energy, ΔE_a is the relative standard error of the calculated activation energy

based on the Kissinger, Augis–Bennett/Boswell and FWO methods, correspondently, which are quite close. The relative standard error of the estimated values ranges from about 9.25 to 9.39%. This high value of activation energy is due to the high temperature required for the complete decomposition of gadolinium oxycarbonate derivatives before the formation of $GdFeO_3$, as discussed earlier (See Section "Differential scanning calorimetry and thermogravimetric analysis"). In accordance with the Kissinger method, the pre-exponential factor has an average value of about 1.62×10^{60} min^{-1}.

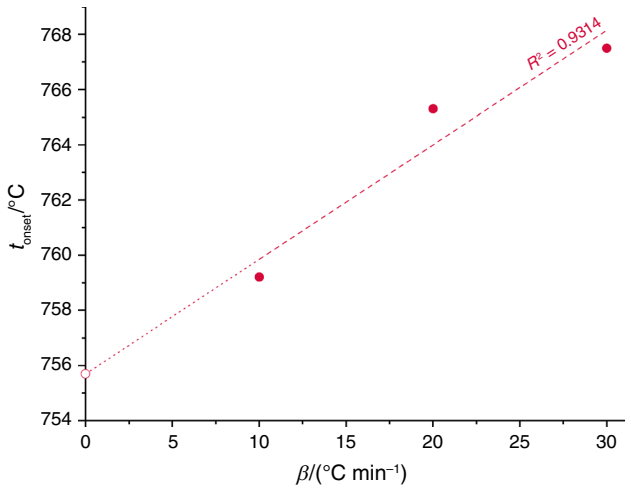

Fig. 5 Dependence of the onset temperature of the formation of nanocrystalline $GdFeO_3$ on the heating rate

True onset temperature of the formation of nanocrystalline $GdFeO_3$

The values of the onset temperature of the exothermic effect of $GdFeO_3$ formation previously determined from the DSC curves (Table 2) are found to be about 759, 765 and 768 °C at a heating rate of 10, 20 and 30 °C min^{-1}, respectively. Therefore, the temperature at which nanocrystalline $GdFeO_3$ begins to form increases with increasing heating rate. To found the true onset temperature of the formation of nanocrystalline $GdFeO_3$, i.e., at a heating rate of 0 °C min^{-1}, the dependence of t_{onset} on β was plotted, and as a result, a straight line was obtained (Fig. 5). By extrapolating the resulting straight line to the y-axis (where $\beta = 0$ °C min^{-1}), the true onset temperature of the formation of nanocrystalline $GdFeO_3$ was found to be about 756 °C, which is quite close to the temperature of 750 °C used in our previous works [25–30].

Powder X-ray diffraction

The diffractograms of the products of heat treatment of the co-precipitated gadolinium and iron(III) hydroxides in the temperature range of 650–850 °C for 4 h are presented in Fig. 6. According to these diffraction patterns, the heat-treated product obtained at a temperature of 650 °C is X-ray amorphous, whereas the products that underwent heat treatment at a temperature of 800 °C and higher are pure-phase crystalline samples and consist of orthorhombic gadolinium orthoferrite (o-$GdFeO_3$) (ICSD 27278, space group

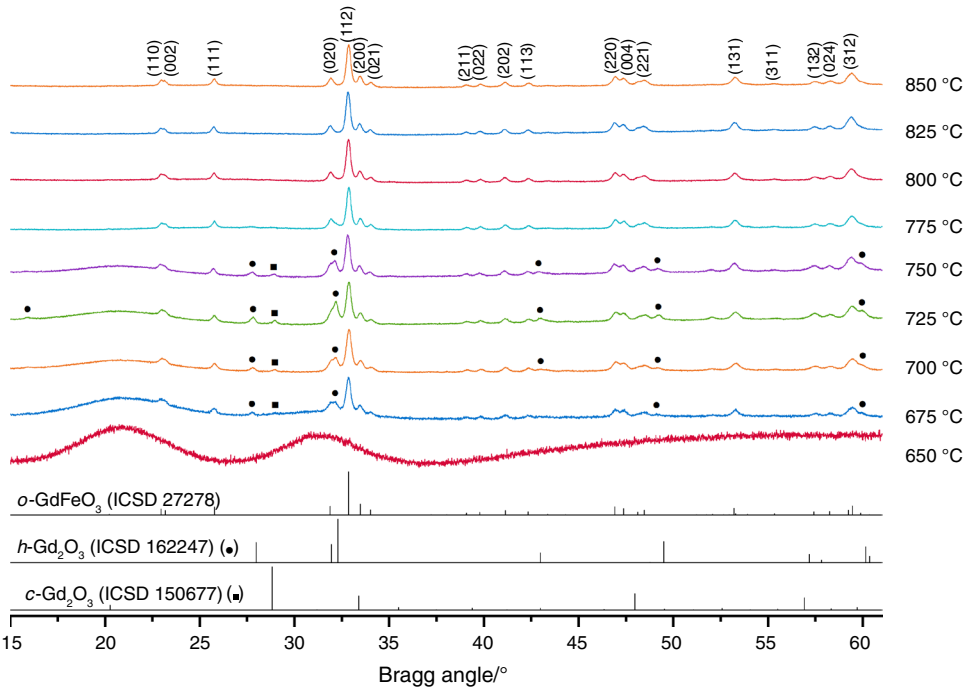

Fig. 6 Powder X-ray diffraction patterns of the heat-treated products of the co-precipitated hydroxides. The peak bars indicate the positions of the reflections of the ICSD structures used in the Rietveld refinement. The Miller indices presented belong to o-$GdFeO_3$

62: *Pbnm*). On the other hand, the X-ray phase analysis of the heat-treated products obtained in the temperature range of 675–775 °C shows that, in addition to *o*-$GdFeO_3$, they also contain other crystalline phases that, apparently, can be associated with hexagonal gadolinium oxide (*h*-Gd_2O_3) (ICSD 162247, space group 164: *P*-3*m*1) and cubic gadolinium oxide (*c*-Gd_2O_3) (ICSD 150677, space group 206: *Ia*-3). Along with these three crystalline phases, the last-mentioned products also contain X-ray amorphous phases, as seen from the amorphous halo in the Bragg angle range of ~ 15.2–27.2°. These phases include amorphous iron(III) oxide (*am*-Fe_2O_3), amorphous gadolinium oxide (*am*-Gd_2O_3) and/or amorphous gadolinium oxycarbonate derivatives "*am*-$Gd_2O_{3-x}(CO_3)_x$". The estimated results of mass fractions of the X-ray amorphous and crystalline phases in all heat-treated products are presented in Fig. 7.

In accordance with Fig. 7, with an increase in the treatment temperature from 650 to 700 °C, the mass fraction of X-ray amorphous phases sharply decreases (from 100% at 650 to ~ 31% at 700 °C), while the mass fraction of *o*-$GdFeO_3$ sharply increases (from 0 at 650 to ~ 61% at 700 °C). This can be explained by the formation of *o*-$GdFeO_3$ as a result of the reaction of *am*-Fe_2O_3 and *am*-Gd_2O_3 at temperatures of 675–700 °C. This primary pathway of $GdFeO_3$ formation is independent of the decomposition of gadolinium oxycarbonate derivatives.

On the other hand, the mass fractions of *h*-Gd_2O_3 and *c*-Gd_2O_3 progressively increase with an increase in the treatment temperature up to 725 °C (reaching a maximum of ~ 13% for *h*-Gd_2O_3 and ~ 1.5% for *c*-Gd_2O_3), above which they begin to decrease gradually and completely disappear at a temperature of 800 °C. It is well known

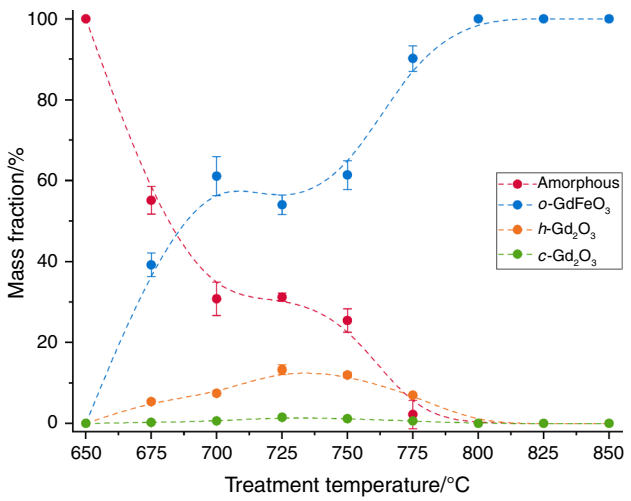

Fig. 7 Mass fractions of the X-ray amorphous phases "*am*-Fe_2O_3, *am*-Gd_2O_3, *am*-$Gd_2O_{3-x}(CO_3)_x$" and crystalline phases (*o*-$GdFeO_3$, *h*-Gd_2O_3, *c*-Gd_2O_3) in the heat-treated products of the co-precipitated hydroxides

that under normal conditions, gadolinium oxide may exist in cubic (C-type, space group 206: *Ia*-3) or monoclinic (B-type, space group 12: *C*2/*m*) forms, whereas the hexagonal form (A-type, space group 164: *P*-3*m*1), at ambient pressure, is only stable at very high temperatures (more than 2443 K/ ~ 2170 °C) [42, 43]. However, the formation of *h*-Gd_2O_3 in the products heat treated in the temperature range of 675–775 °C is most likely related to the presence of gadolinium oxycarbonate derivatives, which, if they were crystalline, could have a hexagonal form that is more stable than other crystalline forms, e.g., the hexagonal form of $Gd_2O_2CO_3$ is more stable than its tetragonal and monoclinic forms [44]. Based on this assumption and the results obtained, in the temperature range of 675–725 °C, gadolinium oxycarbonate derivatives progressively decompose with the formation of CO_2 and *h*-Gd_2O_3, which then transforms to the form stable in the synthesis conditions, *c*-Gd_2O_3, which, at temperatures of 725–775 °C, reacts with *am*-Fe_2O_3 to form *o*-$GdFeO_3$. This is the secondary pathway of $GdFeO_3$ formation that depends on the decomposition of gadolinium oxycarbonate derivatives. It should be noted that the formation of *o*-$GdFeO_3$ as a result of the reaction of *am*-Fe_2O_3 and *h*-Gd_2O_3, i.e., without the transformation of *h*-Gd_2O_3 to *c*-Gd_2O_3, may be possible, but there is no clear evidence for this, especially since the mass fraction of *c*-Gd_2O_3 is less than the mass fraction of *h*-Gd_2O_3 in all heat-treated products containing both of these phases, which indicates that the $GdFeO_3$ formation along this pathway occurs with the participation of *c*-Gd_2O_3 consumed. Besides, since the last stage of decomposition of gadolinium oxycarbonate derivatives proceeds at a temperature of ~ 756–758, as follows from the DTG curves (Table 1, effect 7), *h*-Gd_2O_3 can be formed even above the temperature of 725 °C; however, we cannot observe this on the diffractograms of the products heat treated at temperatures of 750–775 °C, most likely because above the temperature of 725 °C, *h*-Gd_2O_3 transforms to *c*-Gd_2O_3 which then reacts with *am*-Fe_2O_3 faster than *h*-Gd_2O_3 is produced from the decomposition of gadolinium oxycarbonates derivatives. Similarly, the $GdFeO_3$ formation along this pathway can begin below the temperature of 725 °C, but in this case, the reaction of *c*-Gd_2O_3 (and perhaps *h*-Gd_2O_3) with *am*-Fe_2O_3 is slower than the production of *h*-Gd_2O_3 from the decomposition of gadolinium oxycarbonate derivatives. The obtained results are in good agreement with the results of DSC, according to which the exothermic effect of $GdFeO_3$ formation is observed at a temperature of ~ 764–772 °C (Table 1, effect 8).

Figure 8 illustrates the proposed mechanism for the formation of nanocrystalline $GdFeO_3$ synthesized, i.e., by ultrasound-assisted co-precipitation, as follows from the DSC–TGA and PXRD data.

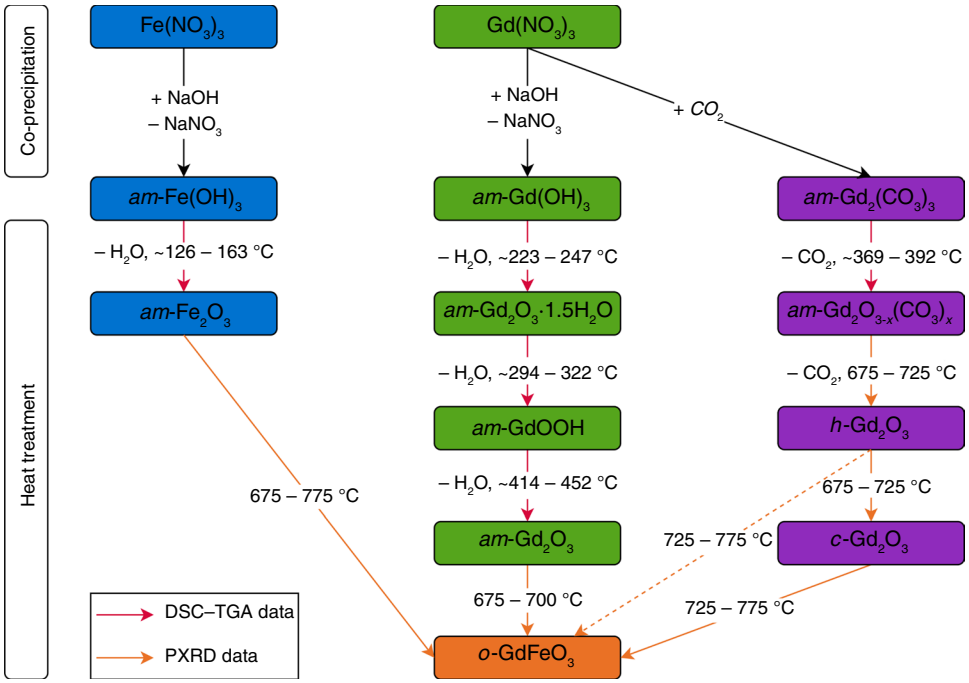

Fig. 8 Mechanism of formation of nanocrystalline $GdFeO_3$ via heat treatment of co-precipitated hydroxides

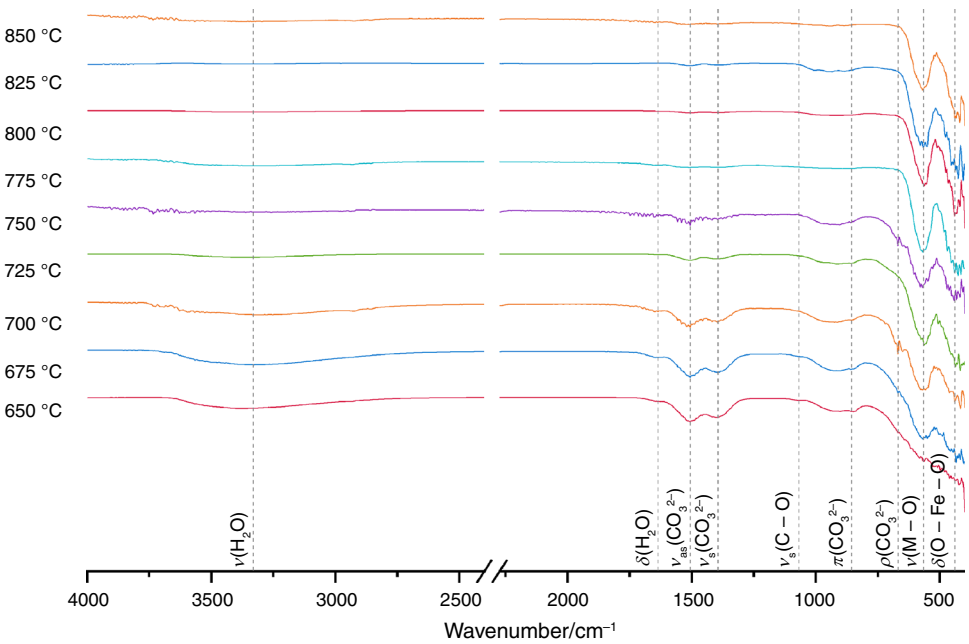

Fig. 9 FTIR spectra of the heat-treated products of the co-precipitated hydroxides (M = Gd^{3+}, Fe^{3+}). The absorption bands corresponding to atmospheric CO_2 in the wavenumber range of ~ 2275–2400 cm^{-1} were omitted to facilitate comparison

Fourier-transform infrared spectroscopy

The FTIR spectra of the products of heat treatment of the synthesized sample of co-precipitated gadolinium and iron(III) hydroxides in the temperature range of 650–850 °C for 4 h are presented in Fig. 9. The wavenumbers of the absorption bands that correspond to the main vibrations in the obtained FTIR spectra of the products that underwent heat treatment in the temperature range of 650–775 °C and their assignment are summarized in Table 4.

Table 4 Assignment of the absorption bands corresponding to the main vibrations in the FTIR spectra of the products heat treated up to 775 °C

Band no	Wavenumber/cm^{-1}						Assignment
	650 °C	675 °C	700 °C	725 °C	750 °C	775 °C	
1	3385	3329	3313	3383	3256	3324	$\nu(H_2O)$
2	1637	1637	1637	1637	1636	1637	$\delta(H_2O)$
3	1507	1507	1507	1507	1507	1508	$\nu_{as}(CO_3^{2-})$
4	1398	1396	1396	1393	1396	1391	$\nu_s(CO_3^{2-})$
5	1066	1072	1088	1066	1045	1071	ν_s(C–O)
6	849	857	857	859	859	857	$\pi(CO_3^{2-})$
7	668	668	670	670	670	664	$\rho(CO_3^{2-})$
8	566	569	570	564	570	569	ν(M–O), M = Gd^{3+}, Fe^{3+}
9	–	435	441	438	444	441	δ(O–Fe–O)

The broad absorption band in the region of high wavenumbers centered at ~ 3256–3385 cm^{-1} (band 1) is a consequence of the overlapping of asymmetric and symmetric stretching vibrations of water "$\nu(H_2O)$", which is physically adsorbed on the surface of the samples during their storage and/or preparation for investigation [28]. The absorption band of the bending vibration of physically adsorbed water "$\delta(H_2O)$" is observed at ~ 1636–1637 cm^{-1} (band 2). The bands observed at ~ 1507–1508 cm^{-1} (band 3) and at ~ 1391–1398 cm^{-1} (band 4) can be attributed to the asymmetric "$\nu_{as}(CO_3^{2-})$" and symmetric "$\nu_s(CO_3^{2-})$" stretching vibrations of carbonate groups, respectively, whereas the bands observed at ~ 1045–1088 cm^{-1} (band 5), at ~ 849–859 cm^{-1} (band 6) and at ~ 664–670 cm^{-1} (band 7) may be assigned to the symmetric stretching vibration of the C–O bond "ν_s(C–O)", the out-of-plane bending "$\pi(CO_3^{2-})$" and rocking "$\rho(CO_3^{2-})$" vibrations of carbonate groups, correspondently [45]. The band observed at ~ 564–570 cm^{-1} (band 8) can be attributed to the stretching vibrations of the Gd–O bond "ν(Gd–O)" and the Fe–O bond "ν(Fe–O)" in the Gd–O–Fe and Fe–O–Fe systems [46], while the band observed at ~ 435–444 cm^{-1} (band 9) may be assigned to the O–Fe–O bending vibration "δ(O–Fe–O)" in octahedral FeO_6 groups [31]. The last-mentioned absorption band (band 9) is practically absent in the FTIR spectrum of the product heat treated at a temperature of 650 °C, which is X-ray amorphous as followed from the PXRD results (see Section "Powder X-ray diffraction").

As can be seen from Fig. 9, the intensity of the asymmetric and symmetric stretching vibrations of carbonate groups (Table 4, bands 3 and 4) on the normalized FTIR spectra in the wavenumber range of ~ 1260–1625 cm^{-1} gradually decreases with an increase in heating temperature to become practically negligible at a temperature of 800 °C. The relative mass percentages of gadolinium oxycarbonate derivatives in the products that underwent heat treatment at temperatures up to 800 °C, estimated based on the integrated intensity of these vibrations, are presented in Fig. 10. The mass fractions of h-Gd_2O_3 in these heat-treated products, previously estimated using the PXRD

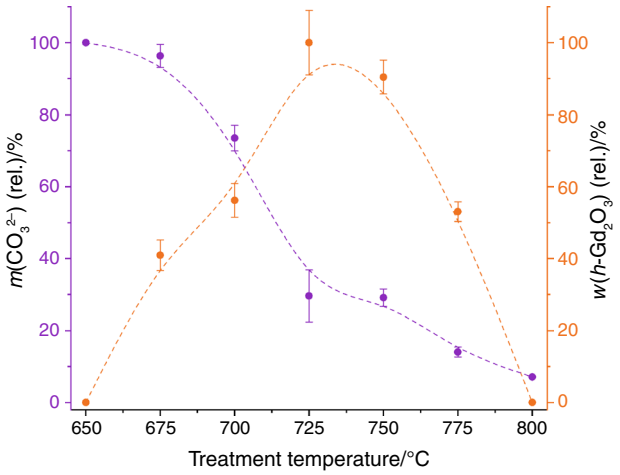

Fig. 10 Relative mass percentages of gadolinium oxycarbonate derivatives in the products heat treated at temperatures up to 800 °C according to the FTIR data (purple) and relative mass fractions of h-Gd_2O_3 in these products as followed from the PXRD results (orange). "Relative (rel.)" here means that the values are calculated relative to the maximum

data, were recalculated as percentages of the maximum and presented in the same figure for comparison.

The results presented in Fig. 10 are in good agreement with our assumption that gadolinium oxycarbonate derivatives progressively decompose with the formation of h-Gd_2O_3 up to the temperature of 725 °C, above which the mass fraction of h-Gd_2O_3 begins to decrease due to the formation of o-$GdFeO_3$ along with the secondary pathway, i.e., with the participation of c-Gd_2O_3 (see Section "Powder X-ray diffraction"). Above the temperature of 725 °C, gadolinium oxycarbonate derivatives continue to decompose gradually, but, as we discussed earlier, h-Gd_2O_3 then transforms to c-Gd_2O_3 which reacts with am-Fe_2O_3 faster than h-Gd_2O_3 is produced; therefore, we observe not an increase but a decrease in the mass fraction of h-Gd_2O_3. At a temperature of 800 °C, h-Gd_2O_3 completely disappears and gadolinium oxycarbonate derivatives become practically negligible.

Carbonate content in gadolinium oxycarbonate derivatives

To estimate the carbonate content in gadolinium oxycarbonate derivatives, i.e., to estimate the values of x in the formula $Gd_2O_{3-x}(CO_3)_x$ at different temperatures, we used the TGA data at temperatures of 700, 725 and 750 °C at different heating rates (10–30 °C min^{-1}) as well as the PXRD data for the products that underwent heat treatment at these temperatures, which include only am-Fe_2O_3 and am-$Gd_2O_{3-x}(CO_3)_x$ as amorphous phases. As discussed earlier, at temperatures of 675–700 °C, am-Fe_2O_3 reacts with am-Gd_2O_3 to form o-$GdFeO_3$ along the primary pathway (see Section "Powder X-ray diffraction"); therefore, the product heat treated at a temperature of 675 °C still contains am-Gd_2O_3, the presence of which complicates the calculation (the unnormalized diffraction pattern of this product shown in Fig. S2 confirms that, at a treatment temperature of 675 °C, o-$GdFeO_3$ is not fully crystallized in comparison with the products heat treated at higher temperatures). As for the product heat treated at a temperature of 775 °C, the relative mass percentage of gadolinium oxycarbonate derivatives is rather small (Fig. 10), which may also affect the calculation results.

According to the EDXS results, the average Gd:Fe atomic ratio is about 1.000:1.003, which is maintained during heat treatment (see Section "Energy-dispersive X-ray spectroscopy"); therefore, the average Gd:Fe molar ratio can be considered equal to 1:1 in all heat-treated products, which means that the amounts in moles (n) of gadolinium and iron are equal (Eq. 8).

$$n_{Gd} = n_{Fe} \tag{8}$$

The amounts in moles of gadolinium and iron in the selected heat-treated products can be determined from Eqs. 9 and 10, respectively.

$$n_{Gd} = n_{o-GdFeO_3} + 2n_{h-Gd_2O_3} + 2n_{c-Gd_2O_3} + 2n_{Gd_2O_{3-x}(CO_3)_x} \tag{9}$$

$$n_{Fe} = n_{o-GdFeO_3} + 2n_{am-Fe_2O_3} \tag{10}$$

Substituting Eqs. 9 and 10 in Eq. 8 and rearranging, we can determine the amount in moles of $Gd_2O_{3-x}(CO_3)_x$ (Eq. 11).oxycarbonate derivatives, one mole

$$n_{Gd_2O_{3-x}(CO_3)_x} = n_{am-Fe_2O_3} - n_{h-Gd_2O_3} - n_{c-Gd_2O_3} \tag{11}$$

Since the amount of a substance in moles is equal to its mass (m) divided by its molar mass (M), Eq. 11 can be written as shown in Eq. 12.

$$\frac{m_{Gd_2O_{3-x}(CO_3)_x}}{M_{Gd_2O_{3-x}(CO_3)_x}} = \frac{m_{am-Fe_2O_3}}{M_{Fe_2O_3}} - \frac{m_{h-Gd_2O_3}}{M_{Gd_2O_3}} - \frac{m_{c-Gd_2O_3}}{M_{Gd_2O_3}} \tag{12}$$

The molar mass of gadolinium oxycarbonate derivatives can be determined as a function of x from Eq. 13.

$$M_{Gd_2O_{3-x}(CO_3)_x} = M_{Gd_2O_3} + x \cdot M_{CO_2} \tag{13}$$

Dividing both sides of Eq. 12 by the mass of the sample at a temperature of t (m_t) and considering that the mass of a phase divided by the sample mass at a certain temperature is equal to the mass fraction of that phase (w) at that temperature, Eq. 12 is converted to Eq. 14.

$$\frac{w_{Gd_2O_{3-x}(CO_3)_x}}{M_{Gd_2O_3} + x \cdot M_{CO_2}} = \frac{w_{am-Fe_2O_3}}{M_{Fe_2O_3}} - \frac{w_{h-Gd_2O_3}}{M_{Gd_2O_3}} - \frac{w_{c-Gd_2O_3}}{M_{Gd_2O_3}} \tag{14}$$

The mass fraction of am-Fe_2O_3 in the selected samples can be determined from the estimated mass fraction of amorphous phases (w_{amorph}) by subtracting the mass fraction of the other amorphous phase, $Gd_2O_{3-x}(CO_3)_x$, as shown in Eq. 15.

$$w_{am-Fe_2O_3} = w_{amorph} - w_{Gd_2O_{3-x}(CO_3)_x} \tag{15}$$

Substituting Eq. 15 in Eq. 14 and rearranging, we can determine the mass fraction of gadolinium oxycarbonate derivatives in the investigated samples as a function of x (Eq. 16).

Table 5 TGA and PXRD data used in the estimation of carbonate content in gadolinium oxycarbonate derivatives and the results obtained

β/(°C min^{-1})	t/°C	TGA data		PXRD data			x	$w(Gd_2O_{3-x}(CO_3)_x)$/%
		m_t/mg	$m(CO_2)$/mg	w_{amorph}/%	$w(h\text{-}Gd_2O_3)$/%	$w(c\text{-}Gd_2O_3)$/%		
10	700	8.81975	0.08035	30.79	7.46	0.62	0.41	19.18
	725	8.79854	0.05915	31.20	13.28	1.53	0.33	17.34
	750	8.75725	0.01786	25.42	12.01	1.19	0.12	13.67
20	700	9.14450	0.09254	30.79	7.46	0.62	0.46	19.21
	725	9.11790	0.06594	31.20	13.28	1.53	0.36	17.35
	750	9.08782	0.03586	25.42	12.01	1.19	0.24	13.73
30	700	8.97771	0.09617	30.79	7.46	0.62	0.49	19.23
	725	8.95311	0.07157	31.20	13.28	1.53	0.40	17.37
	750	8.92627	0.04473	25.42	12.01	1.19	0.31	13.76

$$w_{Gd_2O_{3-x}(CO_3)_x} = \frac{\left[w_{amorph} \cdot M_{Gd_2O_3} - \left(w_{h-Gd_2O_3} + w_{c-Gd_2O_3}\right) \cdot M_{Fe_2O_3}\right] \cdot \left(M_{Gd_2O_3} + x \cdot M_{CO_2}\right)}{M_{Gd_2O_3} \cdot \left(M_{Fe_2O_3} + M_{Gd_2O_3} + x \cdot M_{CO_2}\right)} \quad (16)$$

In accordance with the decomposition equation for gadolinium oxycarbonate derivatives, one mole of $Gd_2O_{3-x}(CO_3)_x$ decomposes with the release of x mole of CO_2, and a mass of $m(Gd_2O_{3-x}(CO_3)_x)$ decomposes with the release of a mass of $m(CO_2)$; therefore, using chemical arithmetic, we can write Eq. 17.

$$m_{Gd_2O_{3-x}(CO_3)_x} \cdot x \cdot M_{CO_2} = m_{CO_2} \cdot M_{Gd_2O_{3-x}(CO_3)_x} \quad (17)$$

Since the mass of $Gd_2O_{3-x}(CO_3)_x$ at a certain temperature, as mentioned above, is equal to its mass fraction multiplied by the sample mass at that temperature, Eq. 17 can be written as shown in Eq. 18.

$$w_{Gd_2O_{3-x}(CO_3)_x} \cdot m_t \cdot x \cdot M_{CO_2} = m_{CO_2} \cdot \left(M_{Gd_2O_3} + x \cdot M_{CO_2}\right) \quad (18)$$

Substituting Eq. 16 in Eq. 18, rearranging and solving for x, we obtain the required equation (Eq. 19).

$$x = \frac{m_{CO_2} \cdot M_{Gd_2O_3} \cdot \left(M_{Fe_2O_3} + M_{Gd_2O_3}\right)}{M_{CO_2} \cdot \left[M_{Gd_2O_3} \cdot \left(m_t \cdot w_{amorph} - m_{CO_2}\right) - m_t \cdot M_{Fe_2O_3} \cdot \left(w_{h-Gd_2O_3} + w_{c-Gd_2O_3}\right)\right]} \quad (19)$$

Using Eq. 19, the carbonate content in gadolinium oxycarbonate derivatives in the investigated samples can be estimated. At different heating rates (10–30 °C min^{-1}), the sample mass at a temperature of t (m_t), where t = 700, 725 and 750 °C, was determined from the TGA curves (Fig. 2b). In addition, the mass of CO_2 included in the sample at a temperature of t "$m(CO_2)$", i.e., its mass that will be released upon the complete decomposition of gadolinium oxycarbonate derivatives in this sample, was also determined using the TGA data as the difference between the sample mass at each temperature (m_t) and the sample mass at the end (completion) of mass loss on the TGA curve (m_{end}). The mass fractions of the amorphous phases (w_{amorph}), h-Gd_2O_3 "$w(h\text{-}Gd_2O_3)$" and c-Gd_2O_3 "$w(c\text{-}Gd_2O_3)$" at each investigated temperature were previously estimated based on the PXRD data (Fig. 7). The TGA and PXRD data used and the calculation results are summarized in Table 5. The dependences of x in $Gd_2O_{3-x}(CO_3)_x$ on temperature at different heating rates are presented in Fig. 11.

As follows from Fig. 11, the obtained dependences can be described by linear equations with coefficients of determination in the range of 0.9363–0.9999. The extrapolation of these dependences to the temperature of 775 °C shows

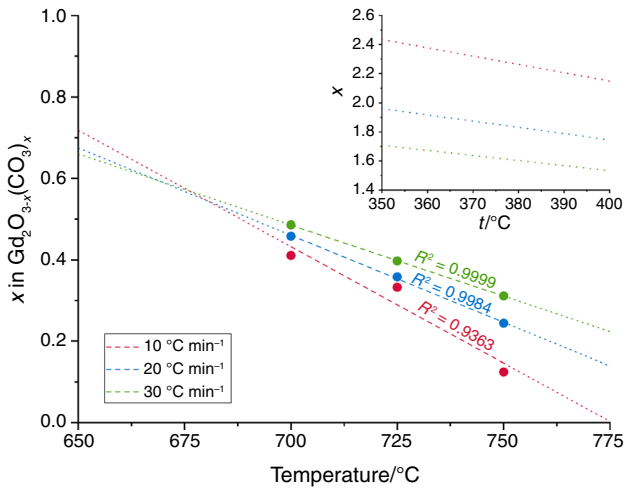

Fig. 11 Dependences of x in the formula of gadolinium oxycarbonate derivatives "$Gd_2O_{3-x}(CO_3)_x$" on temperature (t) at different heating rates. The inset shows the extrapolation of these dependences to the temperature range in which the obtained DSC and DTG curves showed the first stage of gadolinium carbonate decomposition with the formation of an oxycarbonate derivative. R^2 is the coefficient of determination

that x at this temperature is estimated at ~ 0.00–0.22 with an average value of ~ 0.12, which is in good agreement with the PXRD and FTIR results. On the other hand, extrapolating the resulting dependences to the temperature range in which the obtained DSC and DTG curves showed the first stage of gadolinium carbonate decomposition with the formation of an oxycarbonate derivative (Table 1, effect 5), the x value in this derivative may be estimated at ~ 1.56–2.33 with an average value of ~ 1.91. This result is very close to the literature data [33], according to which, at a temperature of ~ 363–370 °C, gadolinium carbonate "$Gd_2(CO_3)_3$" decomposes to gadolinium monooxydicarbonate "$Gd_2O(CO_3)_2$" with the release of CO_2.

Conclusions

In this work, a complex and detailed experimental investigation of the mechanism of formation of $GdFeO_3$ nanocrystals was performed, which shows that the co-precipitated gadolinium and iron(III) hydroxides upon heat treatment undergo a series of physicochemical processes including the dehydration to the corresponding oxides and the decomposition of gadolinium oxycarbonate derivatives prior to the formation of $GdFeO_3$. The PXRD results indicated that the $GdFeO_3$ formation occurs via two pathways: a primary carbonate-independent pathway involving *am*-Gd_2O_3 and a secondary carbonate-dependent pathway involving *h*-Gd_2O_3 and *c*-Gd_2O_3. The FTIR results showed that gadolinium oxycarbonate derivatives gradually decompose with increasing heating temperature to become practically negligible at a temperature of 800 °C. The resulting linear equations for the dependence of x in $Gd_2O_{3-x}(CO_3)_x$ on temperature predict that gadolinium carbonate at a temperature of ~ 266–426 °C decomposes to $Gd_2O(CO_3)_2$ which, at a temperature of ~ 553–601 °C, decomposes to $Gd_2O_2CO_3$, which, in turn, decomposes to Gd_2O_3 at a temperature of ~ 776–839 °C.

Supplementary Information The online version contains supplementary material available at https://doi.org/10.1007/s10973-023-12647-7.

Acknowledgements The study was partially performed using the equipment of the Engineering Center of Saint Petersburg State Institute of Technology.

Authors' contributions Y. Albadi and V. I. Popkov contributed to conceptualization, methodology, validation and formal analysis; Y. Albadi and A. K. Bachina did investigation; A. K. Bachina and V. I. Popkov helped in resources; Y. Albadi did data curation, writing—original draft, visualization and writing—review & editing; V. I. Popkov contributed to writing—review & editing, supervision, project administration and funding acquisition.

Declarations

Conflict of interest The authors do not have relevant financial or non-financial interests to disclose.

References

1. Bamzai KK, Bhat M. Electrical and magnetic properties of some rare earth orthoferrites ($RFeO_3$ where R = Y, Ho, Er) systems. Integr Ferroelectr. 2014;158:108–22.
2. Zhou Z, Guo L, Yang H, Liu Q, Ye F. Hydrothermal synthesis and magnetic properties of multiferroic rare-earth orthoferrites. J Alloys Compd. 2014;583:21–31.
3. Ramu N, Muralidharan R, Meera K, Jeong YH. Tailoring the magnetic and magnetoelectric properties of rare earth orthoferrites for room temperature applications. RSC Adv. 2016;6:72295–9.
4. Nakhaei M, Sanavi KD. Study on structural, magnetic and electrical properties of $ReFeO_3$ (Re= La, Pr, Nd, Sm & Gd) orthoferrites. Physica B Condens Matter. 2021;612: 412899.
5. Warshi MK, Mishra V, Sagdeo A, Mishra V, Kumar R, Sagdeo PR. Structural, optical and electronic properties of $RFeO_3$. Ceram Int. 2018;44:8344–9.
6. Wang Z-Q, Lan Y-S, Zeng Z-Y, Chen X-R, Chen Q-F. Magnetic structures and optical properties of rare-earth orthoferrites $RFeO_3$ (R = Ho, Er, Tm and Lu). Solid State Commun. 2019;288:10–7.
7. Sultan K, Samad R, Islam SAU, Habib MZ, Ikram M. Effect of rare earth ions (R = Pr, Eu and Ho) on the structural and electrical properties of orthoferrites. J Electron Mater. 2019;48:6003–7.
8. Yafarova LV, Chislova IV, Zvereva IA, Kryuchkova TA, Kost VV, Sheshko TF. Sol–gel synthesis and investigation of catalysts on the basis of perovskite-type oxides $GdMO_3$ (M = Fe, Co). J Solgel Sci Technol. 2019;92:264–72. https://doi.org/10.1007/s10971-019-05013-3.
9. Niu X, Li H, Liu G. Preparation, characterization and photocatalytic properties of $REFeO_3$ (RE=Sm, Eu, Gd). J Mol Catal A Chem. 2005;232:89–93.
10. Li L, Wang X, Lan Y, Gu W, Zhang S. Synthesis, photocatalytic and electrocatalytic activities of wormlike $GdFeO_3$ nanoparticles by a glycol-assisted sol-gel process. Ind Eng Chem Res. 2013;52:9130–6. https://doi.org/10.1021/ie400940g.
11. Zhang Y, Zheng A, Yang X, He H, Fan Y, Yao C. Cubic $GdFeO_3$ particle by a simple hydrothermal synthesis route and its photoluminescence and magnetic properties. CrystEngComm. 2012;14:8432.
12. Niu X, Du W, Du W. Preparation, characterization and gas-sensing properties of rare earth mixed oxides. Sens Actuators B Chem. 2004;99:399–404.
13. Söderlind F, Fortin MA, Petoral RM Jr, Klasson A, Veres T, Engström M, et al. Colloidal synthesis and characterization of ultrasmall perovskite $GdFeO_3$ nanocrystals. Nanotechnology. 2008;19: 085608.
14. Pinho SLC, Amaral JS, Wattiaux A, Duttine M, Delville M-H, Geraldes CFGC. Synthesis and characterization of rare-earth orthoferrite $LnFeO_3$ nanoparticles for bioimaging. Eur J Inorg Chem. 2018;2018:3570–8. https://doi.org/10.1002/ejic.201800468.
15. Athar T, Vishwakarma SK, Bardia A, Khan AA. Super paramagnetic iron oxide and gadolinium ($FeGdO_3$) nanopowder synthesized by hydrolytic approach passes high level of biocompatibility and MRI-based dual contrast property for competent molecular imaging and therapeutic interventions. Biomed

Phys Eng Express. 2016;2:025010. https://doi.org/10.1088/2057-1976/2/2/025010.
16. Deka S, Saxena V, Hasan A, Chandra P, Pandey LM. Synthesis, characterization and in vitro analysis of α-Fe_2O_3–$GdFeO_3$ biphasic materials as therapeutic agent for magnetic hyperthermia applications. Mater Sci Eng C. 2018;92:932–41.
17. Abiev RSh, Almjasheva OV, Popkov VI, Proskurina OV. Microreactor synthesis of nanosized particles: the role of micromixing, aggregation, and separation processes in heterogeneous nucleation. Chem Eng Res Des. 2022;178:73–94.
18. Mariyappan V, Keerthi M, Chen S-M, Jeyapragasam T. Nanostructured perovskite type gadolinium orthoferrite decorated RGO nanocomposite for the detection of nitrofurantoin in human urine and river water samples. J Colloid Interface Sci. 2021;600:537–49.
19. Ateia EE, Hussein B, Singh C, Okasha N. Study of physical properties of Co substituted $GdFeO_3$ orthoferrites and evaluation of their antibacterial activity. J Inorg Organomet Polym Mater. 2020;30:4320–8.
20. Santhosh BS, Yashas SR, Kumara Swamy N, Shivaraju HP. Application of non-hierarchical gadolinium ortho-ferrite nanostructure for LED-driven photocatalytic mineralization of doxycycline hydrochloride. J Mater Sci: Mater Electron. 2022;33:11676–86.
21. Tang P, Hu Y, Lin T, Jiang Z, Tang C. Preparation of nanocrystalline $GdFeO_3$ by microwave method and its visible-light photocatalytic activity. Integr Ferroelectr. 2014;153:73–8. https://doi.org/10.1080/10584587.2014.902720.
22. Sivakumar M, Gedanken A, Bhattacharya D, Brukental I, Yeshurun Y, Zhong W, et al. Sonochemical synthesis of nanocrystalline rare earth orthoferrites using $Fe(CO)_5$ precursor. Chem Mater. 2004;16:3623–32. https://doi.org/10.1021/cm049345x.
23. Mathur S, Shen H, Lecerf N, Kjekshus A, Fjellvåg H, Goya GF. Nanocrystalline orthoferrite $GdFeO_3$ from a novel heterobimetallic precursor. Adv Mater. 2002;14:1405–9.
24. Lone IH, Khan H, Jain AK, Ahmed J, Ramanujachary KV, Ahmad T. Metal-organic precursor synthesis, structural characterization, and multiferroic properties of $GdFeO_3$ nanoparticles. ACS Omega. 2022;7:33908–15.
25. Albadi Y, Martinson KD, Shvidchenko AV, Buryanenko IV, Semenov VG, Popkov VI. Synthesis of $GdFeO_3$ nanoparticles via low-temperature reverse co-precipitation: the effect of strong agglomeration on the magnetic behavior. Nanosyst Phys Chem Math. 2020;11:252–9.
26. Albadi Y, Sirotkin AA, Semenov VG, Abiev RS, Popkov VI. Synthesis of superparamagnetic $GdFeO_3$ nanoparticles using a free impinging-jets microreactor. Russ Chem Bull. 2020;69:1290–5. https://doi.org/10.1007/s11172-020-2900-x.
27. Popkov VI, Albadi Y. The effect of co-precipitation temperature on the crystallite size and aggregation/agglomeration of $GdFeO_3$ nanoparticles. Nanosyst Phys Chem Math. 2021;12:224–31.
28. Albadi Y, Ivanova MS, Grunin LY, Martinson KD, Chebanenko MI, Izotova SG, et al. The influence of co-precipitation technique on the structure, morphology and dual-modal proton relaxivity of $GdFeO_3$ nanoparticles. Inorganics (Basel). 2021;9:39.
29. Albadi Y, Abiev RS, Sirotkin AA, Martinson KD, Chebanenko MI, Nevedomskiy VN, et al. Physicochemical and hydrodynamic aspects of $GdFeO_3$ production using a free impinging-jets method. Chem. Eng. Process.: Process Intensif. 2021;166: 108473.
30. Albadi Y, Ivanova MS, Grunin LY, Makarin RA, Komlev AS, Chebanenko MI, et al. Ultrasound-assisted co-precipitation synthesis of $GdFeO_3$ nanoparticles: structure, magnetic and MRI contrast properties. Phys Chem Chem Phys. 2022;24:29014–23.
31. Prakash BJ, Rudramadevi BH, Buddhudu S. Analysis of ferroelectric, dielectric and magnetic properties of $GdFeO_3$ nanoparticles. Ferroelectr Lett Sect. 2014;41:110–22. https://doi.org/10.1080/07315171.2014.956020.
32. Tugova EA, Karpov ON. Nanocrystalline perovskite-like oxides formation in Ln_2O_3–Fe_2O_3–H_2O (Ln = La, Gd) systems. Nanosyst Phys Chem Math. 2014;5:854–60.
33. Popkov VI, Tugova EA, Bachina AK, Almyasheva OV. The formation of nanocrystalline orthoferrites of rare-earth elements $XFeO_3$ (X = Y, La, Gd) via heat treatment of coprecipitated hydroxides. Russ J Gen Chem. 2017;87:2516–24. https://doi.org/10.1134/S1070363217110020.
34. Natarajan M, Secco EA. Anisotropic conductivity and phase transformation studies in potassium chromate crystals. Can J Chem. 1974;52:2436–8.
35. Glushko VP, editor. Thermal constants of substances. handbook in 10 Issues. Issue 8. Part 1. Tables of accepted values. Moscow: USSR Academy of Sciences. All-Union Institute of Scientific and Technical Information. Institute for High Temperatures; 1978.
36. Kissinger HE. Reaction kinetics in differential thermal analysis. Anal Chem. 1957;29:1702–6.
37. Augis JA, Bennett JE. Calculation of the Avrami parameters for heterogeneous solid state reactions using a modification of the Kissinger method. J Therm Anal. 1978;13:283–92.
38. Boswell PG. On the calculation of activation energies using a modified Kissinger method. J Therm Anal. 1980;18:353–8.
39. Ozawa T. A new method of analyzing thermogravimetric data. Bull Chem Soc Jpn. 1965;38:1881–6.
40. Flynn JH, Wall LA. A quick, direct method for the determination of activation energy from thermogravimetric data. J Polym Sci B. 1966;4:323–8.
41. Zhang X. Applications of kinetic methods in thermal analysis: a review. Eng Sci. 2021;14:1–13.
42. Zinkevich M. Thermodynamics of rare earth sesquioxides. Prog Mater Sci. 2007;52:597–647.
43. Zhang FX, Lang M, Wang JW, Becker U, Ewing RC. Structural phase transitions of cubic Gd_2O_3 at high pressures. Phys Rev B. 2008;78: 064114.
44. Ge W, Li Z, Lei Z, Chen T, Fu Z, Peng R, et al. Synthesis of hexagonal phase $Gd_2O_2CO_3$: Yb^{3+}, Er^{3+}upconversion nanoparticles via SiO_2 coating and Nd^{3+} doping. CrystEngComm. 2015;17:5702–9.
45. Gaspar RDL, Mazali IO, Sigoli FA. Particle size tailoring and luminescence of europium(III)-doped gadolinium oxide obtained by the modified homogeneous precipitation method: Dielectric constant and counter anion effects. Colloids Surf A Physicochem Eng Asp. 2010;367:155–60.
46. Sai Vandana C, Hemalatha Rudramadevi B. Effect of Cu^{2+} substitution on the structural, magnetic and electrical properties of gadolinium orthoferrite. Mater Res Express. 2018;5(4): 046101. https://doi.org/10.1088/2053-1591/aab7a8